Chinese Chemical Letters 36 (2025) 109776

Contents lists available at ScienceDirect

Chinese Chemical Letters

journal homepage: www.elsevier.com/locate/cclet

Carbon interconnected microsized Si film toward high energy room temperature solid-state lithium-ion batteries

Xin Li[a,1], Ling Zhang[c,1], Yunyan Fan[a,1], Shaojing Lin[a], Yong Lin[a], Yongsheng Ying[a], Meijiao Hu[a], Haiying Gao[a], Xianri Xu[a], Zhongbiao Xia[a], Xinchuan Lin[a], Junjie Lu[b], Xiang Han[b,*]

[a] School of Information Engineering, Fujian Business University, Fuzhou 350012, China
[b] College of Materials Science and Engineering, Co-Innovation Center of Efficient Processing and Utilization of Forest Resources Nanjing Forestry University, Nanjing 210037, China
[c] College of Artificial Intelligence, Yango University, Fuzhou 350015, China

ARTICLE INFO

Article history:
Received 22 January 2024
Revised 22 February 2024
Accepted 14 March 2024
Available online 16 March 2024

Keywords:
Lithium-ion battery
Solid-state electrolyte
Silicon anode
Carbon coating
Interphase

ABSTRACT

Solid-state batteries (SSBs) with high-capacity Si anodes have been regarded as one of the most promising candidates to meet the large scale energy storage and electrical vehicles due to its intrinsic safety and potential high energy density. However, Si suffers from poor electrical conductivity and huge volume change and particles fracture during lithiaiotn and delithiation, which induces low practical energy density. In addition, the SSBs are often operated at high temperature due to the poor physical contact and huge resistance between Si and solid-state electrolyte (SSE). To improve the bulk electronic/ionic conductivity of Si and its interfacial compatibility with SSE, herein, a binder free and self-supporting Si/C film was developed. The monolithic carbon not only enhance the electric conductivity but also release huge stress during lithiation and delithiation. In addition, paired with the flexible and soft poly(vinylidene fluoride)-*co*-hexafluoropropylene (PVDF-HFP) and $Li_{1.3}Al_{0.3}Ti_{1.7}(PO_4)_3$ (LATP) solid-state electrolyte, a LiF-rich and electrochemical stable solid-electrolyte interphase (SEI) layer is *in-situ* engineered. The fast bulk and interfacial ionic transportation as well as the mechanical integrity of MSi enable high performance SSBs at room temperature. As a result, high specific capacity of 2137 mAh/g with an initial Coulombic efficiency of 83.2% is obtained at a rate of 0.5 A/g. Even at a high rate of 3 A/g, the specific capacity is 1793 mAh/g. At a rate of 1 A/g, the Si/C anode delivers a long cycling performance over 500 cycles while maintains a capacity of 1135 mAh/g. This work provides a new strategy that combines charge transfer kinetics and interfacial chemistry design toward high energy density Si-based SSBs.

Energy storage devices, such as lithium-ion batteries (LIBs), plays a crucial role in the wide spread of clean energy storage and electrical vehicles (EVs). Electrolyte plays a crucial role in the ionic transport and interfacial chemistry of cathodes and anodes, however, traditional liquid carbonate-based electrolytes suffer from safety issues due to its intrinsic flammable properties [1–3]. Replacing liquid electrolyte by nonflammable solid-state electrolytes (SSEs) have been considered as a basic strategy that resolve the safety problems of LIBs [4–10]. At the same time, applying high specific capacity active materials could significantly improve the specific energy density of LIBs, such as Si anode shows a high theoretical specific capacity of ~4200 mAh/g (*vs.* $Li_{22}Si_5$) [11–17], which is ten times higher than that of commercial graphite anode (~370 mAh/g). In addition, Si shows low working potential (~0.4 V *vs.* Li^+/Li) and natural abundance advantages [18,19]. Building Si-based solid-state batteries will substantially improve the total energy density of LIBs.

It should be noted that the fluidity of SSEs is very poor and could not wet the surface of active materials, especially for the particle configuration with large surface area [20,21]. As a result, the charge transfer kinetics including electrons and lithium ions are retarded and cause huge resistance. On the other hand, the side reaction mechanism and electrochemical stability between Si and SSEs is not clear, which will seriously affect the cycling stability [22–24]. To resolve the above-mentioned issues, conductive materials such as carbon and metals are coated on the Si particles. The surface coating noy only enhance the carrier transport but also help

* Corresponding author.
E-mail address: hanxiang@njfu.edu.cn (X. Han).
[1] These authors contribute equally to this work.

https://doi.org/10.1016/j.cclet.2024.109776
1001-8417/

to accommodate the volume expansion [25]. Doping or designing composite alloys are also demonstrated to improve the conductivity and release the mechanical stress during lithiation and delithiation. LiSi alloy was successfully fabricated by self- and was demonstrated as flexible buffer and conductive framework for microsized Si anode [26]. Li-Si-hard carbon was also fabricated, which serves as an ionic-electronic-conductive network composed of plastically deformable Li-rich phases ($Li_{15}Si_4$ and LiC_6) that enlarges active area and relieves stress concentration is created in the anode, leading to improved electrode kinetics and mechanical stability [27]. SiO_x combined with manipulated electrolyte design which serves to aid formation of robust passivation layers on the anode [28]. Incorporating some content of SSEs has been considered as an effective way to enhance the inter-particles conductivity [29]. However, the direct contact between the particles and SSE will cause unwanted side reactions, especially for high surface area nano Si particles. To maintain compact interfacial physical contact between Si and SSE, a high temperature (>50 °C) or physical pressure (several hundred MPa) applied, which is a big obstacle for practical application. Regarding this, a substantial way should be carried out, that could not only engineer the architecture at electrode scale but also design three-dimensional ionic-electronic-conductive network at the interface. In addition, how to further reduce the bulk or interfacial resistance and manipulate the solid-state battery at room temperature to meet the practical requirements still remain challenging.

Herein, a novel three-dimensional carbon interconnected micrometer Si (MSi-C) structure was designed, among which the carbon not only serves as binder that reserve the Si as a monothetic film, but also functions as an ionic-electronic-conductive network. The unique architecture was fabricated by simply carbonization of PAN-coated MSi. The interfacial binding nature and conductivity of C significantly improves during thermal heating process, that further enhance the mechanical and conductivity of the anode. Furthermore, taking advantage of poly(vinylidene fluoride)-*co*-hexafluoropropylene (PVDF-HFP)/$Li_{1.3}Al_{0.3}Ti_{1.7}(PO_4)_3$ solid-state electrolyte, a LiF-rich SEI layer was detected, which should enhance the interfacial mechanical and ionic conductive property. Taking advantage of the conductive network and superior interfacial property, high electrochemical performance was obtained even at room temperature. For example, the MSi-C anode delivers a specific capacity of 2142 mAh/g at 0.5 A/g and still remains 1793 mAh/g at 3 A/g, which is 84% of that at 0.5 A/g. For the long-term test at 1 A/g, a 500-cycle life is obtained and remained 1135 mAh/g. More importantly, the high-rate performance is achieved at room temperature and without any pressure. Our work shed light on the design of Si anode and manipulating interfacial resistance toward high energy density solid-state battery.

The micron-sized silicon (MSi) powders with an average diameter of ~1.5 μm were purchased from Xuzhou Lingyun Silicon Industry Co., Ltd. The MSi powders were directly used without any treatment. For the preparation of MSi-C electrode, the MSi powders and polyacrylonitrile (PAN) solution (10 wt% dissolved in *N*,*N*-dimethylformamide, DMF) were mixed in a weight ratio of 5:5 and ball-milled 2 h to form a slurry. The mixed slurry was spread onto copper foil and dried for 12 h in a vacuum drying oven at 80 °C to evaporate the residual DMF. The MSi-PAN on copper foil was cut into small discs with a diameter of 12 mm and then calcined at 700 °C for 2 h under Ar/H_2 (5%) atmosphere to obtain the MSi/C electrode. The active material mass loading including MSi and C is around 0.5 mg/cm^2.

PVDF-HFP with an average M_w of ~400,000 was purchased from Sigma-Aldrich. NASICON-type LATP with a diameter of ~200 nm was purchased from synthesized by from Guangdong Canrd New Energy Technology Co., Ltd. For the preparation of PVDF-HFP/LATP composite SSE, 0.6 g PVDF-HFP powders, 0.6 g lithium bis(trifluoromethane sulfonimide) (LiTFSI) and 0.2 g LATP nanoparticles were dissolved in DMF and stirred at 60 °C for 24 h. After then, the slurry was cast on a clean glass plate, PVDF-HFP/LATP solid-state composite SSE film was fabricated after dried in a vacuum oven at 80 °C for 24 h. The thickness of as-prepared PVDF-HFP/LATP film is ~50 μm.

The crystal structure of the as-synthesized LATP, MSi, MSi-C and SPE were characterized by X-ray diffraction (XRD) (Cu K_α, λ ~0.15406 nm). A field-emission scanning electron microscope (FESEM, JSM-7600F) equipped with energy-dispersive X-ray spectroscopy (EDS) (FEI Titan F20) was applied to observe the surface and cross-sectional morphology of the MSi particles MSi-C electrode and SPE. The surface chemistry of MSi-C anode before and after cycling was analyzed by X-ray photoelectron spectroscopy (XPS) (Thermo Scientific K_α spectrometer).

All the electrochemical performances were tested in CR 2025-type coin cells, which were assembled in a glovebox filled with high purity Ar (H_2O < 1 ppm, O_2 < 1 ppm). The solid polymer electrolyte used was PVDF-HFP/LATP. To assemble the solid-state half-cell, the PVDF-HFP/LATP SPE serves as separator and electrolyte between PS-Ag-C electrode and lithium metal. The coil cells were measured between 0.005 and 1.5 V on a LAND CT2001A battery test instrument. For a full cell, $LiFePO_4$ (LFP) was chose as cathode with a mass ratio of 12:1 to MSi/C anode. The receipt of the cathode contains 80 wt% LFP, 10 wt% carbon black and 10 wt% PVDF. Cyclic voltammetry (CV) with a scan rate of 0.2 mV/s was performed on a Bio-Logic VSP-300 electrochemical workstation. Electrochemical impedance spectroscopy (EIS) tests were carried out between 7 MHz and 0.1 Hz with an AC amplitude of 10 mV to record the impedance variation of MSi-C anode during cycling. The electrochemical cycling performances of all solid-state cells were performed at room temperature.

Ionic conductivity (σ) of LATP/PVDF-HFP SSE was calculated based on the following formula (Eq. 1):

$$\sigma = \frac{L}{RS} \tag{1}$$

where L is the thickness of solid polymer electrolyte; R is the high-frequency intercept obtained from the electrochemical impedance spectroscopy (EIS); S is the surface area of the electrode. Usually, a stainless steel symmetrical electrode is sandwiched with SPE to form a 2025 coin-type half-cell, which is tested by the AC impedance and potentiostatic chronoamperometry. For the AC impedance test, the frequency range is set as 0.01 Hz−7 MHz, and the amplitude of the voltage is set as 10 mV. The DRT transformation of EIS spectra was run in the MATLAB GUI toolbox.

Mircosized Si particles were chosed as the starting materials due to its high tap density, low surface area and low cost. As shown in Fig. 1a, the diameter of the MSi is between 1 μm and 2 μm, and shows a flake configuration. After carbon coating, as shown in Fig. 1b, the MSi particles were embedded in the network of carbonized PAN film. During the thermal heating process, a thin layer of amorphous is coated on the surface of MSi and should have strong interaction with each other. The chemical interaction is covalent Si-N-C bond [30], which is expected to improve the adhesion and mechanical property of MSi/C composite. In this unique configuration, the carbon film serves as electronic additives that facilitate fast electron pathway and binder separate MSi particles as well. In the XRD patterns of MSi-C (Fig. 1c), the diffraction peaks corresponding to Si and Cu were observed [21], suggesting the crystalline nature of MSi. As demonstrated in our previous paper, interfacial $CuSi_x$ alloy may form [31]. No diffraction peak of graphite detected, implying that the carbon is amorphous. For the Raman spectra of MSi-C in Fig. 1d, a sharp peak at 515 cm^{-1} was detected, which is corresponding to the TO mode of crystalline c-Si [32]. In addition, the D band and G band peaks of amorphous

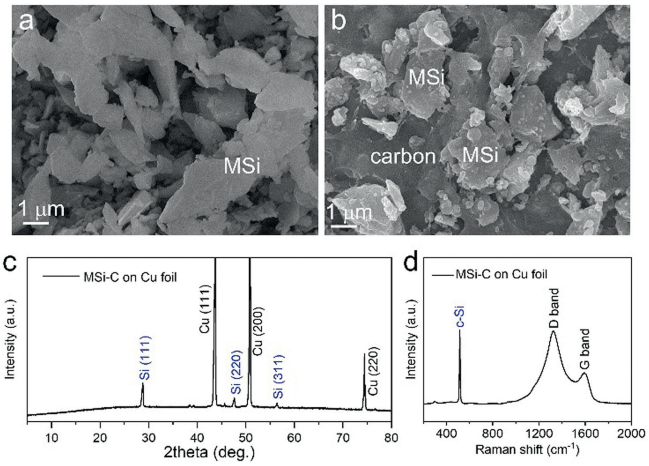

Fig. 1. (a) SEM image of MSi particles. (b) Surface SEM image of MSi-C electrode. (c) XRD patterns of MSi-C anode. (d) Raman spectra of MSi-C anode.

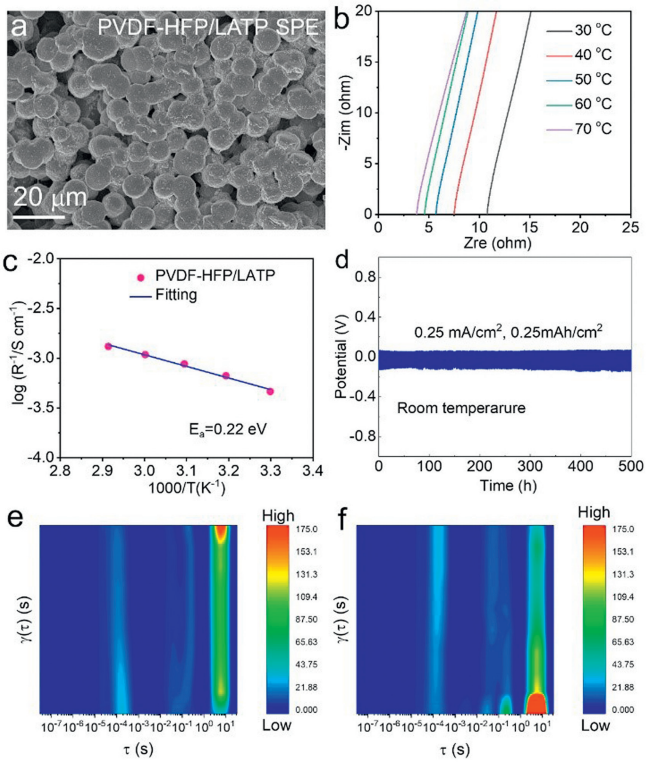

Fig. 2. (a) Surface SEM image of PVHLP SPE. (b) EIS impedance of PVHLP SPE at different temperatures. (c) The Arrhenius plot of PVHLP SPE. (d) The cycling stability of a Li/Li symmetric cell used PVHLP SPE. (e) The DRT transformation of EIS spectra in the first discharge cycle. (f) The DRT transformation of EIS spectra in the first charge cycle.

with a ratio of 2.33 was observed, implying the amorphous nature of the carbon film.

The monothelic and integrated carbon coated MSi netwok shows distinct advantages in a solid-state battery because no carbon and SSE additives added that increasing the contents of active materials. As the same time, the inter-resistance between MSi and SE/C should be neglected, which will further improve the charge transfer kinetics and rate performance. Furthermore, the interacted framework is expected to release the mechanical stress during lithiation and delithiation.

PVDF-HFP and LATP composite solid polymer electrolyte was synthesized and served as separator and electrolyte, donated as PVDF-HFP/LATP (PVHLP). As shown in Fig. 2a, typical balls configuration and some pores of PVDF-HFP polymer matrix was observed, which is caused by phase separation between the polymer and solvent. At a high magnification, as shown in Fig. S1 (Supporting information), it is clearly distinguishing the PVDF-HFP balls and LATP nanoparticles on the surface. The XRD patterns of PVDF-HFP/LATP is shown in Fig. S2 (Supporting information), demonstrating the crystalline nature of LATP nanoparticles and PVDF-HFP polymer. The thickness of the PVHLP SPE is ~50 μm, a thin SPE layer is expected to improve the energy density of SSBs. The impedance of PVHLP at different temperatures is shown in Fig. 2b, the calculated ionic conductivity of the SPE is 4.6×10^{-4}, 6.7×10^{-4}, 8.8×10^{-4}, 1.1×10^{-3}, and 1.3×10^{-3} S/cm at 30, 40, 50, 60, and 70 °C, respectively. The activation energy for PVHLP was evaluated to be 0.22 eV (Fig. 2c) based on the Arrhenius equation [33]. The high ionic conductivity at low temperatures such as 30 °C is enabled by the polymer chains based on DMF-PVDF interactions. Because the trace amount of residual polar DMF solvent combined with high dielectric constant (ε_r, 8–12) of the PVDF polymer facilitates dissociation of Li salt to form $[Li(DMF)_x]^+$ solvation structures [34]. In addition, the high concentration of lithium salt (LiTFSI), which induces the formation of abundant contact ion pairs (one Li^+ binding with one FSI^-, CIPs) and aggregates (one Li^+ binding with two or above FSI^-, AGGs). The newly formed $[Li(DMF\text{-}FSI_x)]^+$ solvation shell, as a result, reduces the activation energy barrier and improves the ionic conductivity at room temperature. The anion-rich solvation structure induces form inorganic-rich and mechanical robust interfacial solid-state interphases. Consequently, as shown in Fig. 2d, the PVHLP SPE exhibits superior stability against Li metal, at room temperature, for a current density of 0.25 mA/cm^2 and an area capacity of 0.25 mAh/cm^2, the Li-Li symmetric cell could stable cycle over 500 h without obvious polarization voltage increasement. As shown in Fig. S3 (Supporting information), the polarization voltage remains stable during long time test, for example, the value is 52, 53 and 70 mV at 100, 200 and 500 h, respectively. The favorable lithium ion transport kinetics and good electrochemical stability of PVHLP SPE is expected to enable high performance cycling performance of Si based electrodes.

To estimate the interfacial property and impedance on the cycling performance, *in-situ* EIS during the first discharge-charge processes was carried out. Typically, all the plots comprise of two semicircles (Fig. S4 in Supporting information), the first one at high frequency corresponding to the SEI impedance (R_{SEI}), and the second one at low frequency corresponding to the charge transfer resistance (R_{ct}), among which the R_{SEI} is larger than R_{ct}. During the lithiation process, based on the equivalent circuit in Fig. S5 (Supporting information), both R_{SEI} and R_{ct} decreases, for example, the R_{SEI} varies from 64 Ω to 33 Ω. The enhanced kinetics may be the following reasons, firstly, Li_xSi alloy has good ionic/electronic conductivity than pristine Si, which counts for the reduced energy barrier between SE and MSi-C. Secondly, the volume and thickness of MSi-C anode increases during the lithiation process and should induce a mechanical pressure on the interface, enabling condense interfacial physical contact. To get a clearer separation of electrochemical process with different time constant, as shown in Figs. 2e and f, the distribution of Relaxation Times (DRT) model of EIS based on Bayesian ridge regression (also known as Tikhonov regularization) was performed. The computation of the DRT is based on Bayesian ridge regression (also known as Tikhonov regularization). The DRT transformation of EIS spectra was run in the MATLAB GUI toolbox created by Ciucci's research group [35].

To evaluate the electrochemical performance of MSi-C anode in solid-state battery, half cells with Li metal as counter electrode, MSi-C film as working electrode and PVHLP serving as electrolyte. The cross-sectional SEM of MSi-C and SSE was shown in Fig. S6

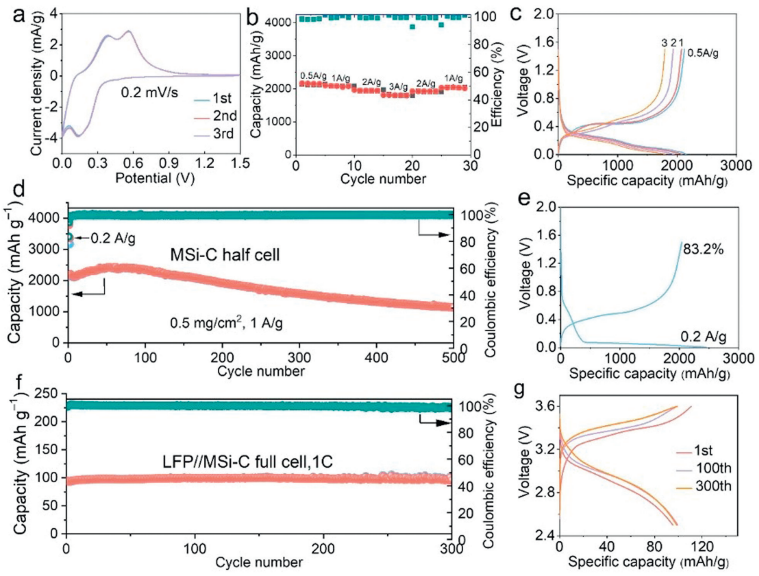

Fig. 3. (a) The CV curves of MSi-C anode in a solid-state cell. (b) The rate performance of MSi-C in a solid-state cell. (c) The corresponding charge-discharge profiles at various currents in (b). (d) The long-term cycling performance of MSi-C. (e) The initial charge-discharge profile of MSi-C anode in (d). (f) The cycling performance of LFP-Si full cell using PVDF-HFP/LATP solid-state electrolyte. (g) The voltage charge-discharge profiles at different cycles in (f).

(Supporting information), intimidate contact without any gap or void were observed between MSi-C and SSE layer, confirming the good interfacial compatibility. As shown in Fig. 3a, the CV curves of MSi-C anode was recorded, for the reduction processes, two typical peaks at 0.03 V and 0.009 V, corresponding to the lithiation processes of amorphous Si [25], because crystalline Si transforms into amorphous Si after initial delithiation process. For the oxidation side, two typical peaks at 0.38 V and 0.56 V were detected, implying the dealloying from amorphous Li_xSi to amorphous Si [36]. The rate performance of MSi-C in a solid-state cell was exhibited in Fig. 3b, at various rates of 0.5, 1, 2 and 3 A/g current density, the specific capacities are 2137, 2078, 1971 and 1793 mAh/g, respectively. Even at a high rate of 3 A/g, the capacity retention is 82.5% compared to that at 0.5 A/g. The voltage profiles at different currents are shown in Fig. 3c, all the profiles at different currents show same shape of amorphous Si and small polarization voltage was observed at a high current density of 3 A/g, demonstrating the fast charge transfer kinetics of MSi-C anode.

To reveal the long-term stability of MSi-C anode in a solid-state battery, as shown in Fig. 3d, a high rate current density of 1 A/g was applied, the MSi-C anode delivers a specific capacity of 2131 mAh/g. During the initial 100 cycles, the cell shows stable cycling performance with a tiny capacity increasement to a value of 2327 mAh/g. After that, the MSi-C electrode shows a slowly decrement and remains a specific capacity of 1135 mAh/g after 500 cycles, corresponding to a capacity retention of 53%. It should be noted that the capacity is obtained at room temperature and without any outer pressure, which is totally different from the oxide and sulfide solid-state electrolytebased batteries. The capacity loss during long-term cycling may be caused by the degraded physical contact induced by huge volume changes during repeated cycles. Fig. 3e shows the initial charge-discharge profile of the MSi-C anode at 0.2 A/g, the long plateau at ~0.1 V observed for the discharge process corresponding to the lithiation of crystalline Si. During the initial charge process, the crystalline Li_xSi alloy transforms into amorphous Li_xSi and then amorphous Si, among which a slope plateau at 0.4–0.6 V observed. The initial Coulombic efficiency is 83.2%, demonstrating the high electrochemical reversibility of MSi-C film in a solid-state cell. A full cell coupled LFP cathode and MSi/C anode was also prepared. The cycling performance was shown in Fig. 3f, at a rate of 1 C, the discharge charge is 95 mAh/g, even after

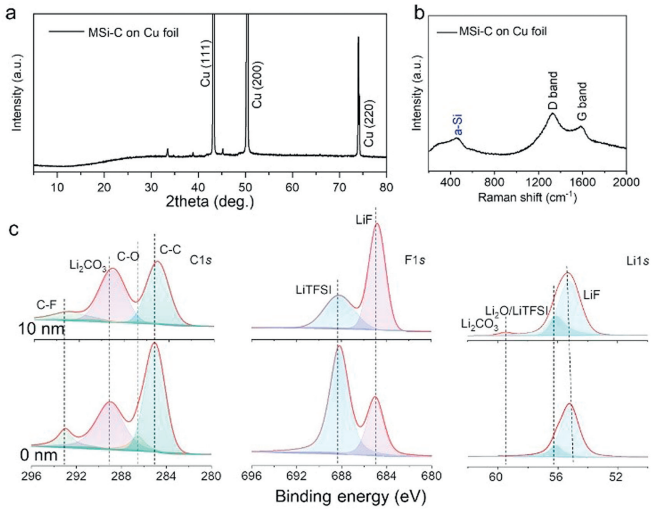

Fig. 4. (a) The XRD diffraction patterns of MSi-C electrode after cycling. (b) The Raman spectrum of MSi-C anode after cycling. (c) The depth XPS analysis of MSi-C anode after cycling for C 1s, F 1s and Li 1s spectra.

300 cycles a capacity of 97 mAh/g was obtained. The charge and discharge voltages were around 3.4 and 3.0 V (Fig. 3g), respectively. The solid-state electrolyte further demonstrates cycling stability in a full cell.

After repeated cycles, the solid-state cells were disassembled and the electrodes were carried out for post analysis. As shown in the XRD patterns in Fig. 4a, only diffraction peaks of Cu were detected, implying that the c-Si transforms into amorphous Si (a-Si) during cycling. For the Raman spectra in Fig. 4b, a broad peak located at ~460 cm^{-1} was assigned to LO and TO mode of a-Si, which is consistent with the XRD results. For the D band and G band of a-C, the ratio decreases to 1.5. As shown in Fig. 4c, the XPS spectra of cycled MSi-C electrode in a solid-state cell was also performed to reveal the SEI information. For the C 1s spectra, besides the peak the C–C and C–O peaks, CO_3^{2-} and $-CF_3$ peaks were also detected, corresponding to the Li_2CO_3 and PVDF-HFP polymer [37], respectively. After a 10 nm etching, the relative contents of

C–C and C-F decreases while the peak intensity of Li_2CO_3, suggesting that the main components of the SEI inner layer is inorganic Li_2CO_3. For F 1s spectra, both LiTFSI and LiF were observed, while the LiF content increases for a 10 nm etching depth. For the Li 1s spectra, LiF was identified as the main component with some Li_2O and Li_2CO_3 for both at the surface and the inner part [38]. It is concluded that the outer surface of SEI comprises PVDF-HFP polymer and the inner part is LiF-rich. The LiF-rich SEI is produced by the high concentration of $TFSI^-$ anions reacting with Li. It has been demonstrated that the Li-CF_3 species mixed in a LiF-rich SEI layer offer a more robust Li passivation layer than an SEI containing LiF alone, which can bring about the high reversibility of Li alloy reactions and enhanced cycling performance of Li/Li^+ redox [39]. The SEI formed in a solid-state cell is confirmed to be inorganic rich and thinner than that in conventional liquid cells.

In summary, to address the low conductivity and unstable issues of Si based anodes, an interconnected mSi-C anodes were designed with monothelic carbon network. The conductive framework not only enhances the electrical conductivity but also helps to release the mechanical stress during cycling. In addition, taking advantage of PVHLP solid-state electrolyte, a stable and LiF-rich SEI layer formed, which contributes to a stable interface between Si and SPE. The improved bulk conductivity, mechanical robust network and stable SEI synergistically high performance in a solid-state cell at room temperature. For example, a high specific capacity of 1135 mAh/g after 500 cycles is achieved, which is 3 times of commercial graphite anode. Evern at a high rate of 3 A/g, the mSi-C anode shows a specific capacity of 1793 mAh/g. This work shed light on the design of Si based anodes toward intrinsic safety and high energy density solid-state batteries.

Declaration of competing interest

The authors declare that they have no known competing financial interests or personal relationships that could have appeared to influence the work reported in this paper.

Acknowledgments

This work was financially supported by the Natural Science Foundation of Fujian Province (No. 2021J01333) and the funding from the Fujian Education Department of China (No. JAT210582).

Supplementary materials

Supplementary material associated with this article can be found, in the online version, at doi:10.1016/j.cclet.2024.109776.

References

[1] A. Manthiram, X. Yu, S. Wang, et al., Nat. Rev. Mater. 2 (2017) 1–16.
[2] Y. Xiao, Y. Wang, S.H. Bo, et al., Nat. Rev. Mater. 5 (2020) 105–126.
[3] X. Han, T. Wu, L.H. Gu, et al., Chin. Chem. Lett. 34 (2023) 107594.
[4] F.Y. Zhang, Y.L. Liang, Z.R. Ye, et al., Chin. Chem. Lett. 35 (2024) 108655.
[5] D.X. Cao, X. Sun, Y.J. Li, et al., Adv. Mater. 34 (2022) 2200401.
[6] Z. Sun, Q. Yin, H. Chen, et al., Interdiscip. Mater. 2 (2023) 635–663.
[7] F. Ren, Z. Liang, W. Zhao, et al., Energy Environ. Sci. 16 (2023) 2579–2590.
[8] J. Gu, H. Zhong, Z. Chen, et al., Chem. Eng. J. 454 (2023) 139923.
[9] Y. Tang, L. Zhang, J. Chen, et al., Energy Environ. Sci. 14 (2021) 602–642.
[10] Q. Dai, J. Yao, C. Du, et al., Adv. Funct. Mater. 32 (2022) 2208682.
[11] X.H. Liu, J.W. Wang, S. Huang, et al., Nat. Nanotechnol. 7 (2012) 749–756.
[12] Y. Yu, H. Gao, J. Zhu, et al., Chin. Chem. Lett. 32 (2021) 203–209.
[13] Y. He, L. Jiang, T. Chen, et al., Nat. Nanotechnol. 16 (2021) 1113.
[14] N. Yang, J. Sun, R. Shao, et al., Cell Rep. Phys. Sci. 3 (2022) 100862.
[15] H. Huo, J. Janek, ACS Energy Lett. 7 (2022) 4005–4016.
[16] X. Xu, Q. Sun, Y. Li, et al., Small 19 (2023) 2302934.
[17] H. Liu, Q. Sun, H. Zhang, et al., Energy Storage Mater. 55 (2023) 244–263.
[18] B. Chen, L. Chen, L. Zu, et al., Adv. Mater. 34 (2022) 2200894.
[19] R. Yu, Y. Pan, Y. Jiang, et al., Adv. Mater. 35 (2023) 2306504.
[20] D.H. Tan, Y.T. Chen, H. Yang, et al., Science 373 (2021) 1494.
[21] Z. Zhao, F. Chen, J. Han, et al., Adv. Energy Mater. 13 (2023) 2300367.
[22] M. Zhao, J. Zhang, C.M. Costa, et al., Adv. Mater. 36 (2024) 2308590.
[23] R.B. Cervera, N. Suzuki, T. Ohnishi, et al., Energy Environ. Sci. 7 (2014) 662–666.
[24] X. Han, L.H. Gu, Z.F. Sun, et al., Energy Environ. Sci. 16 (2023) 5395–5408.
[25] L.H. Gu, J.J. Han, M.F. Chen, et al., Energy Storage Mater. 52 (2022) 547–561.
[26] Z.Y. Zhang, Z. Sun, X. Han, et al., Energy Environ. Sci. 17 (2024) 1061–1072.
[27] W. Yan, Z. Mu, Z. Wang, et al., Nat. Energy 8 (2023) 800–813.
[28] R. Yu, Y. Pan, Y. Jiang, et al., Adv. Mater. 35 (2023) 2306504.
[29] D. Cao, T. Ji, A. Singh, et al., Adv. Energy Mater. 13 (2023) 2203969.
[30] X. Han, H. Chen, X. Li, et al., J. Mater. Chem. 4 (2016) 434–442.
[31] X. Han, H. Chen, J. Liu, et al., Electrochim. Acta 156 (2015) 11–19.
[32] X. Han, Z. Zhang, H. Chen, et al., ACS Appl. Mater. Interfaces 12 (2020) 44840–44849.
[33] X. Han, S. Wang, Y. Xu, et al., Energy Environ. Sci. 14 (2021) 5044–5056.
[34] P. Shi, J. Ma, M. Liu, et al., Nat. Nanotechnol. 18 (2023) 602–610.
[35] T.H. Wan, M. Saccoccio, C. Chen, F. Ciucci, Electrochim. Acta 184 (2015) 483–499.
[36] M.T. McDowell, S.W. Lee, W.D. Nix, Adv. Mater. 25 (2013) 4966–4985.
[37] Z. Zhao, J. Han, F. Chen, et al., Adv. Energy Mater. 12 (2022) 2103565.
[38] J. Chen, X. Fan, Q. Li, et al., Nat. Energy 5 (2020) 386–397.
[39] P. Liang, H. Sun, C.L. Huang, et al., Adv. Mater. 34 (2022) 2207361.